ORIGINAL PAPER

Analysis of Deformed Oxide Layers Grown on Steel

**Lucía Suárez · Pablo Rodríguez-Calvillo ·
Yvan Houbaert · Nelson F. Garza-Montes-de-Oca ·
Rafael Colás**

Abstract   The deformation of the oxide layer grown in ultra low carbon steel was studied by means of electron backscattered diffraction analyses. Samples of the steel were reheated for shorts periods of time at 1050 °C in a chamber designed to obtain thin scale layers before deforming them by plane strain compression at temperatures ranging from 650 to 1050 °C. Microstructural analyses showed that the oxide layer was made almost exclusively of wustite that is ductile when deformed above 900 °C. It is found that wustite develops texture components of the cube and rotated cube type while growing; these components rotate towards ⟨201⟩ {100} components once

L. Suárez · P. Rodríguez-Calvillo
CTM—Technologic Centre, Materials Technology Area, Manresa, Barcelona, Spain
e-mail: lucia.suarez@ctm.com.es

P. Rodríguez-Calvillo
e-mail: pablo.rodriguez@ctm.com.es

L. Suárez · P. Rodríguez-Calvillo
Department of Materials Science and Metallurgical Engineering, Universidad Politécnica
de Cataluña, Barcelona, Spain

Y. Houbaert
Department of Materials Science and Engineering, University of Ghent, Ghent, Belgium
e-mail: Yvan.Houbaert@UGent.be

N. F. Garza-Montes-de-Oca · R. Colás (✉)
Facultad de Ingeniería Mecánica y Eléctrica, Universidad Autónoma de Nuevo León,
Monterrey, Mexico
e-mail: rcolas@mail.uanl.mx

N. F. Garza-Montes-de-Oca
e-mail: nelson.garza@gmail.com

N. F. Garza-Montes-de-Oca · R. Colás
Centro de Innovación, Investigación y Desarrollo en Ingeniería y Tecnología, Universidad
Autónoma de Nuevo León, Monterrey, Mexico

a certain degree of deformation is achieved. Undeformed ferrite close to the oxide layer shows weak $\langle 201 \rangle$ $\{100\}$ components that rotate into weak rotated cube components when the substrate is deformed in the austenite range and to strong $\langle 554 \rangle$ $\{225\}$ components when deformed in ferrite. Rolling trials carried out in an experimental mill showed similar trends.

Introduction

Oxidation is an ever present problem during processing steels at high temperature. The oxide layer formed in the particular case of hot rolling can vary from a few micrometers to a few millimetres. Primary scales are of the order of a few millimetres in thickness, and are normally associated to reheating stages, due to the long times and high temperatures involved; medium size scales, which are known as secondary, are formed as the steel is processed during the roughing stage, as the oxide scale is removed by descaling before rolling, but the scale has time enough to grow during the time between passes. Tertiary scale is encountered during the finishing passes of continuous mills and it is normally thinner than 50 μm, as the transfer bar is descaled prior to be fed into the finishing mill, but the oxide grows and is deformed while the steel is processed [1–3].

The oxide layer found in hot rolled carbon steels is made of three distinct species, which are Fe_2O_3 (hematite), Fe_3O_4 (magnetite) and FeO (wustite). The amount of oxygen decreases from the surface to the metallic interface while the metal decreases in the other direction [4–9]. Wustite occurs with a broad composition range that can be described as $Fe_{1-x}O$, with x varying from 0.04 to 0.17 [10]. The fact that x is always positive implies that wustite is cation-deficient and that the interaction between cations and vacancies is the predominant mechanism of mass transport. The oxide at the temperatures of interest for hot rolling, contains a high proportion of wustite, which is able to deform to a high extent [11–14].

Oxidation studies in low carbon steels are normally limited to light optical microscopy (LOM) or scanning electron microscopy (SEM) [15]. Electron backscattered diffraction (EBSD) is a technique that has been developed in recent years due to the advance in electron beam control in scanning electron microscopes and in the development of software able to characterize and identify the patterns formed by the Kikuchi lines generated by backscattered electrons. This technique has been applied to the study of oxides grown in steels [16–18]. Backscattered diffracted electrons form a series of cones (known as Kossel's cones) that follow Bragg's law and generate the Kikuchi lines when they intersect a phosphorous screen. These patterns can be used to identify the phases and crystallographic orientation of the small volume of sample that interacts with the electron beam [19, 20].

Textures in metals deformed in plane strain compression (of which rolling is the most common process) are represented as being of the type $\langle uvw \rangle$ $\{hkl\}$, which means that the $\{hkl\}$ planes and the $\langle uvw \rangle$ directions of the grains lie parallel to the

plane and the direction of flow of the material (in rolling will be the plane of the sheet and the rolling direction). It is usual to represent texture in the form of pole figures, although the information in pole figures is incomplete and semiquantitative. One way of removing this difficulty is to use the orientation distribution function (ODF), which describes the frequency of occurrence of particular orientations in a three dimensional orientation space. This space is defined by three Euler angles, which constitute a set of three consecutive rotations that bring the crystallographic axes of each crystal grain into coincidence with the specimen axes [19–22]. The most widely accepted notation for describing an ODF is that proposed by Bunge that represents the distribution by means of spherical harmonic functions [21].

A three-dimensional view of Euler space in the Bunge notation is presented in Fig. 1. In this diagram, a series of fibres are indicated. The notations used to identify the directions in rolling and plane strain compression differ; it is normal practice to identify the rolling, normal and transversal that are identified as RD, ND and TD; whereas in plane strain compression these directions will be identified as 1, 3 and 2 [23]. α and γ fibres lie on $\varphi_2 = 45°$ section and contain orientations lying along $\varphi_1 = 0°$ and $\Phi = 55°$, respectively, and correspond to rotations around $\langle 110 \rangle$ // RD and $\langle 111 \rangle$ // ND respectively. η, θ and ζ fibres lie on $\varphi_2 = 0°$ section and correspond to orientations along $\varphi_1 = 0°$, $\Phi = 55°$ and $\varphi_1 = 45°$, respectively, and correspond to rotations of $\langle 100 \rangle$ // RD, $\langle 100 \rangle$ // ND and $\langle 110 \rangle$ // ND respectively.

The aim of this work is to present the results of the analyses conducted on the substrate and on the oxide layer grown on ultra low carbon steel samples. The steels samples were oxidized for short periods of time at 1050 °C before being deformed in plane strain compression at temperatures ranging from 650 to 1050 °C, as these conditions are congruent with those available between descaling and rolling in modern installations.
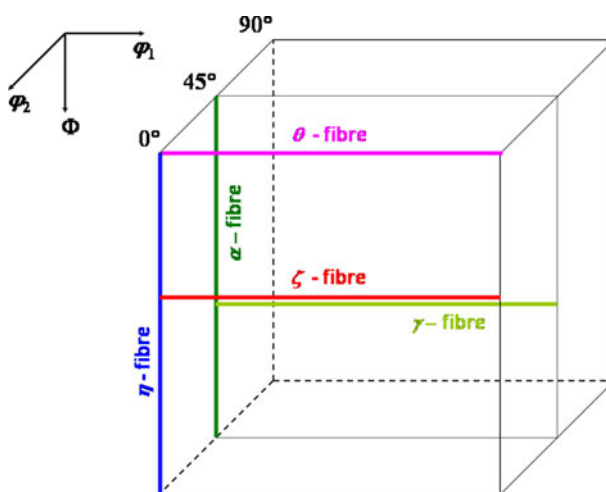

Fig. 1 Representation of the ODF space showing the fibres that occur at φ_2 equal to 0 and 45°

Experimental Procedures

The steel used in the present study was of the ultra low carbon type (0.005 C, 0.078 Si, 0.055 Mn, 0.051 P, 0.027 Cr, 0.036 Al, 0.042 Cu, 0.063 Ti, wt%) that was cut into flat specimens of 100 mm in length by 35 mm in width and 6 mm in thickness. The samples were placed in a chamber designed to form thin scale layers. The chamber was made of mica and is surrounded by an induction coil, which is used to heat-up and control the temperature of the specimen. Nitrogen was used as protective atmosphere within the heating-up period and was replaced by dry air to oxidize the surface of the steel; the small size of the chamber allows for the replacement of either atmosphere in less than 0.1 s. Full details of the chamber can be found elsewhere [24]. The chamber was located within the frame of a servohydraulic testing machine [25–27]. Plane strain compression tests were carried out within the temperature range of 650 to 1050 °C to study the effect of deformation on the oxide layer.

Samples for metallographic examination were prepared with special care. The specimens for LOM and SEM examination were prepared following standard metallographic procedures that included grinding with SiC paper up to grit 1200, followed by polishing with 3 and 1 μm diamond paste. These specimens were lightly etched with a 2% concentration of hydrochloric acid in water. Samples for EBSD analyses had to be polished with colloidal silica (0.035 μm particle size) for long times with decreasing pressure. These studies were conducted in an electron microscope with and LaB_6 filament. The samples were tilted 75° and the analyses were conducted using an acceleration voltage of 20 kV. Texture was represented by the orientation distribution function (ODF) that was calculated according to the notation developed by Bunge applying orthotropic sample symmetry [19–21]. The results of the EBSD analyses are reported in ODF sections of φ_2 equal to 0 and 45°, as different texture fibres occur on them, Fig. 1.

EBSD analyses can be conducted in an automated way by feeding the data related to the crystal symmetry and lattice parameters of the suspected phases into the software used for these means. Ferrite, wustite and magnetite have cubic symmetry with lattice parameters (a) of 0.287, 0.429 and 0.840 nm respectively and hematite crystallizes in a trigonal structure with $a = 0.504$ nm and $b = 1.375$ nm [10, 16].

Additional trials were carried out on material hot rolled with the aid of an experimental mill. The material in this case was interstitial free strip 3 mm in thickness heated up to 1000 °C in a conventional electric furnace. The rolling mill has a water cooling device located at the exit side that allows for the rapid reduction in temperature. Two-single pass reductions (26 and 40%) were given to the strip.

Results

Figure 2a shows a backscattered electron image of the substrate and oxide layer of a sample that was held for 5 s at 1050 °C. Full details on the procedure followed to achieve such a thin oxide layer can be found elsewhere [24]; Fig. 2b shows the
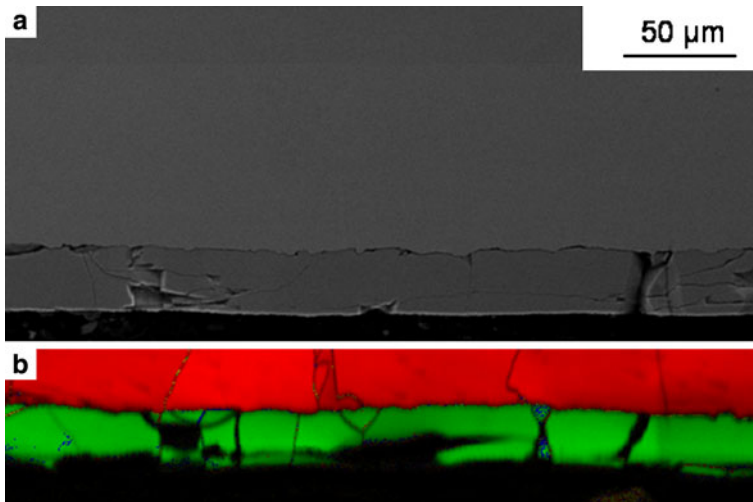
Fig. 2 Backscattered electron image of a specimen oxidized for 5 s at 1050 °C (**a**). EBSD image of the oxide layer and adjacent substrate (**b**)

corresponding EBSD image obtained by the analysis carried out on the sample. The software was used to discriminate between the different phases (ferrite and oxide species) indicating that the oxide layer is made exclusively of wustite. The software set the grain boundaries using the criterion of 15° of miss-orientation between adjacent data points. The EBSD images tend to have a better definition when the material being analyzed is undeformed; therefore, the images of materials that did not have time enough to recrystallize have data points in which the crystal structure was not defined and the software considerer them as missing, leaving them black. This characteristic, called image quality, can be used to discriminate between deformed and recrystallized material.

Figures 3, 4, and 5 show images constructed with the EBSD data of samples oxidized for 5 s at 1050 °C and deformed in plane strain compression at 1050, 950 and 650 °C respectively. The rectangles in Figs. 3a and 4d indicate the areas that appear in Figs. 3a′ and 4d′ at a higher magnification. Difference in tonality between the different grains arises from their orientation. The EBSD analyses carried out on the specimens deformed at 650 °C were limited to samples deformed to low reductions in height as it was found that the oxide layer exhibited a brittle behaviour at this temperature and penetrated into the steel substrate [14]. Figure 6 shows the EBSD images obtained from the samples that were subjected to the rolling trials.

Figure 7 shows the ODF sections at φ_2 equal to 0 and 45° for the oxide (wustite) and the steel substrate (ferrite) of the material that was reheated for 5 s at 1050 °C and was either deformed or subjected to a reduction in 70% height by plane strain compression; these ODF sections corresponds to the EBSD diagrams shown in Fig. 3a, d. Figs. 8 and 9 show ODF sections at φ_2 equal to 0 and 45° for the wustite and ferrite of the material that was reheated at 1050 °C and was left to cool down to
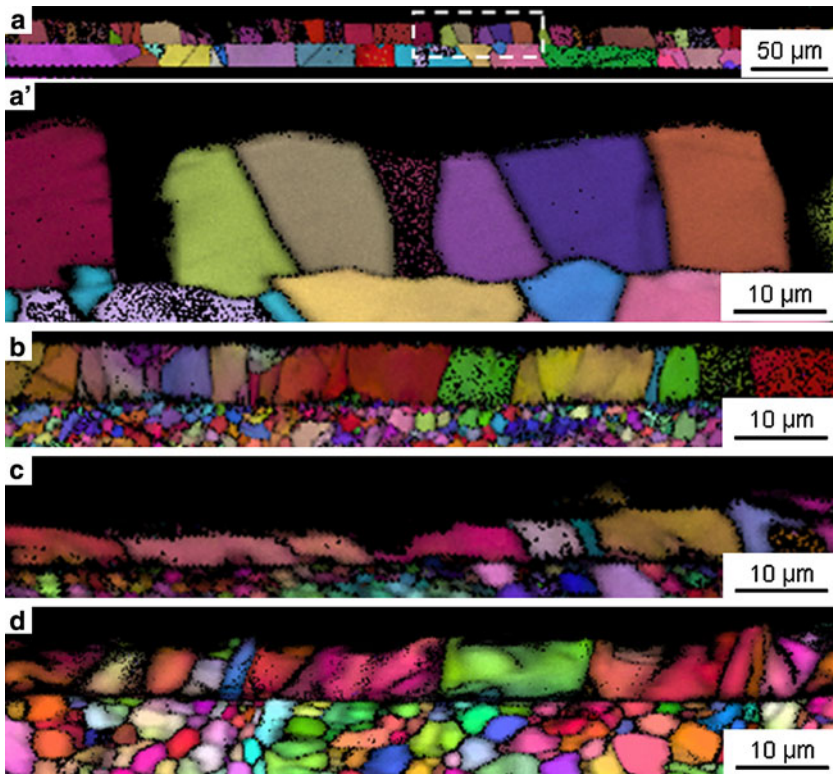
Fig. 3 EBSD images of the material oxidized for 5 s at 1050 °C without deformation (**a**, **a′**) and deformed to 50 (**b**), 60 (**c**) and 70% (**d**) reduction in height

either 950 or 650 °C; Figs. 8a and 9a correspond to the sample left undeformed, whereas Figs. 8b and 9b correspond to the material that was reduced in height to a 70 and a 25% respectively; the corresponding EBSD diagrams are shown as Figs. 4a, d and 5a, b. Figure 10 shows the ODF sections for the material that was reheated at 1000 °C and left undeformed or hot rolled to a 40% reduction in height; the corresponding EBSD diagrams are shown as Figs. 6a, c. The curves shown in Figs. 7, 8, 9 and 10 indicate the relative intensity of the texture components, in which the value of 1 is given to a random (grey) texture.

Discussion

The EBSD images show that the oxide layer is able to resist a high amount of deformation without breaking when the specimens are deformed in the experimental chamber at or above 950 °C, but the integrity of the layer is compromised when the material is deformed below 800 °C [12–14]. The layer grown on the specimens used in the hot rolling trials show a low degree of ductility, and this may be associated to the heat transfer conditions occurring during rolling that cause the reduction of
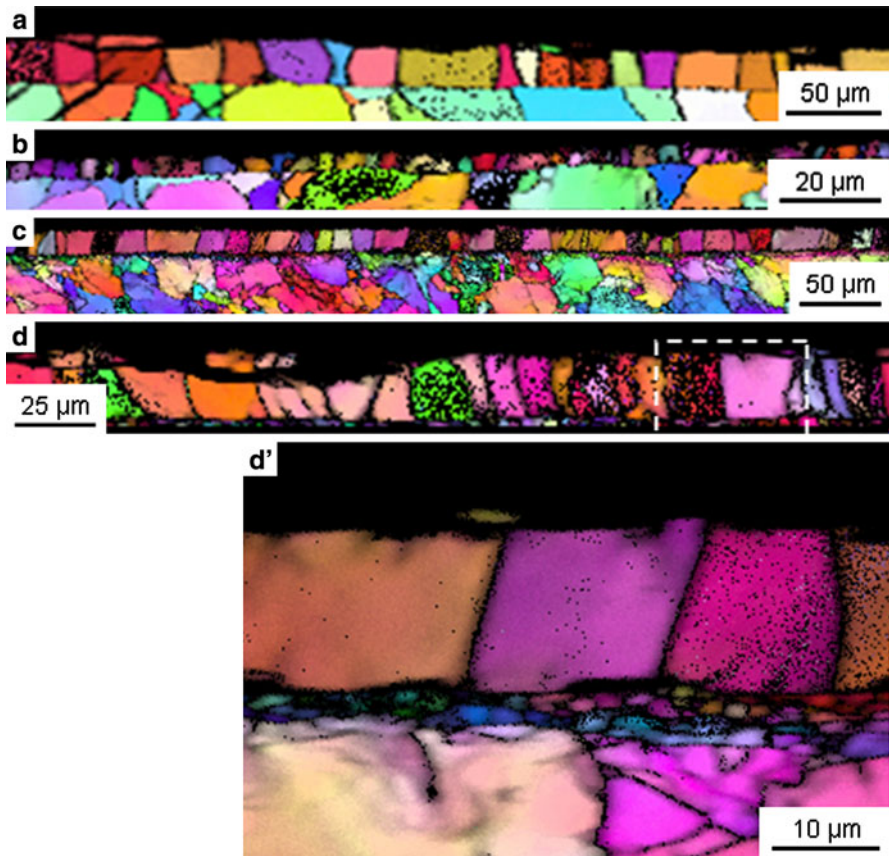
Fig. 4 EBSD images of the material oxidized for 5 s at 1050 °C and cooled to 950 °C without deformation (**a**) and deformed to 10 (**b**), 20 (**c**) and 70% (**d**, **d′**) reduction in height
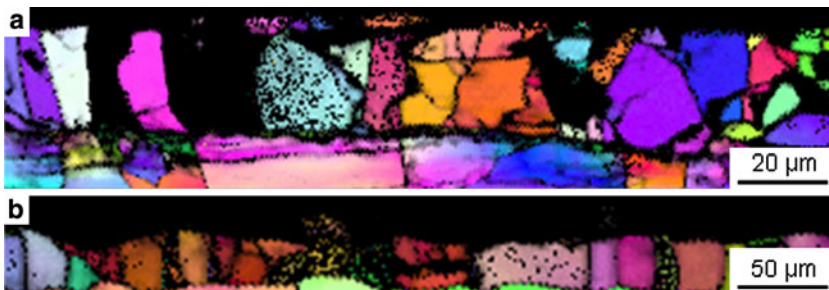

Fig. 5 EBSD images of the material oxidized for 5 s at 1050 °C and cooled to 650 °C without deformation (**a**) and deformed to a 25% (**b**) reduction in height

temperature at the layer [28, 29], and, with it, the reduction in ductility of the oxide layer. The chilling phenomena that affects the ductility of the oxide layer is not observed in the specimens deformed in the experimental chambers as the tooling are
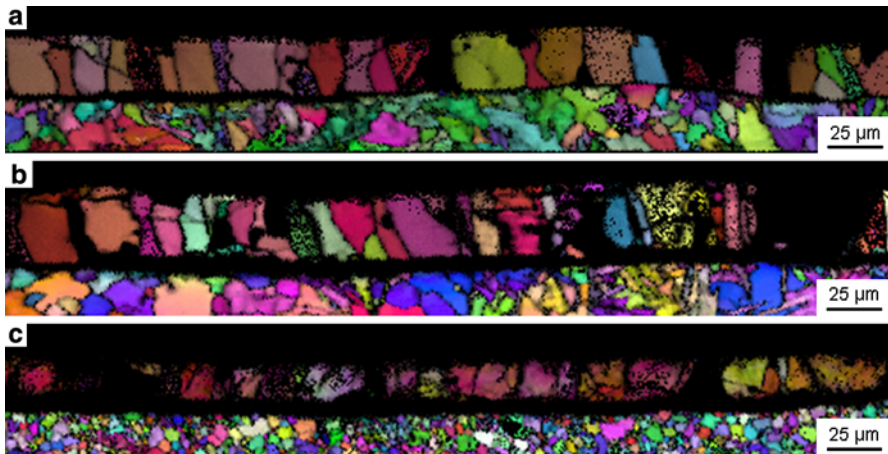
Fig. 6 EBSD images of the material reheated to 1050 °C for rolling (**a**) and after it was subjected to 26 (**b**) and 40% (**c**) reduction in height

heated-up by the induction coil and the deformation takes place almost under isothermal conditions [30].

Another feature that can be observed in Figs. 3, 4 5 and 6 is that the oxide layer grown in the experimental chamber is made exclusively of wustite, Figs. 3, 4 and 5, whereas a thin external layer of magnetite is observed on top of the wustite layer in the sample that was prepared for hot rolling, Fig. 6, and this layer can be caused also by the different heat transfer conditions, as the oxide close to the surface in the rolled samples will be able to cool due to radiation and convection in air and conduction to the work rolls. The reduction in temperature will promote the transformation of wustite into magnetite below 570 °C [10].

The oxide grains within the oxide layer on samples deformed at 950 and 1050 °C appear well defined, implying that the oxide is either undeformed or that it had time enough to recrystallize after deformation, whereas those on samples deformed at 650 °C or hot rolled show a higher degree of distortion within them. The grains in the steel substrate exhibit a similar behaviour; in some cases the grains appear well defined, for example in the undeformed specimens or in the samples deformed at the higher temperatures. Ferrite grains appear refined in some cases, see Fig. 3b–d, and this can be due to the occurrence of dynamic restoration mechanisms taking place while the material is deformed [31, 32].

Figure 11 shows the values of the maximum component of texture obtained by the analyses; these results show that the texture developed within the steel substrate (ferrite) is rather weak, as most values fall within an intensity range of 4–7, The components on wustite are stronger, as most of them fall within the range of 7–12 (only in one case this value is surpassed). Texture in wustite in the undeformed condition tends to lie in the θ-fibre, see Fig. 1; the highest values of texture are found in the samples left undeformed at 950 and 650 °C, Figs. 8a and 9a, in which the $\langle 100 \rangle \{100\}$ cube and $\langle 120 \rangle \{100\}$ rotated cube components are above 11.
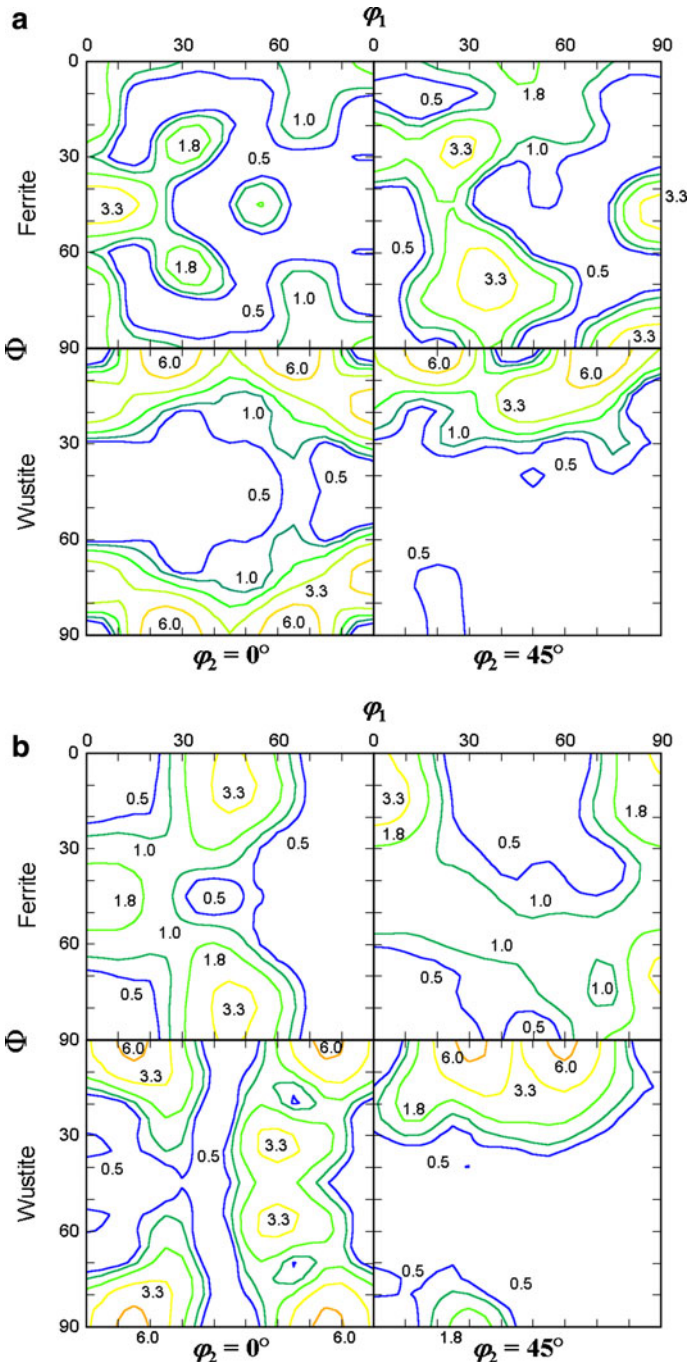
Fig. 7 ODF sections at φ_2 equal to 0 and 45° for wustite and ferrite of the specimens reheated at 1050 °C and left undeformed (**a**) and with a 70% reduction in height (**b**)
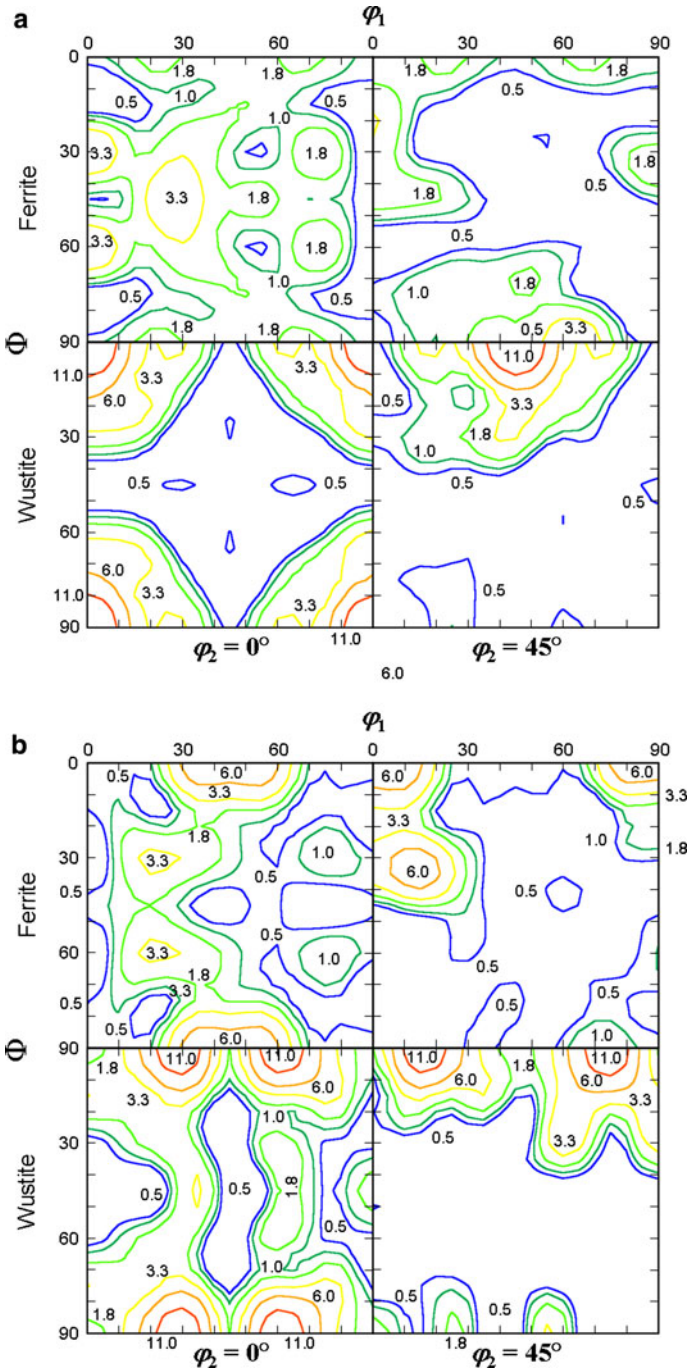
Fig. 8 ODF sections at φ_2 equal to 0 and 45° for wustite and ferrite of the specimens reheated at 1050 °C and cooled to 950 °C that was left undeformed (**a**) and deformed to a 70% reduction in height (**b**)
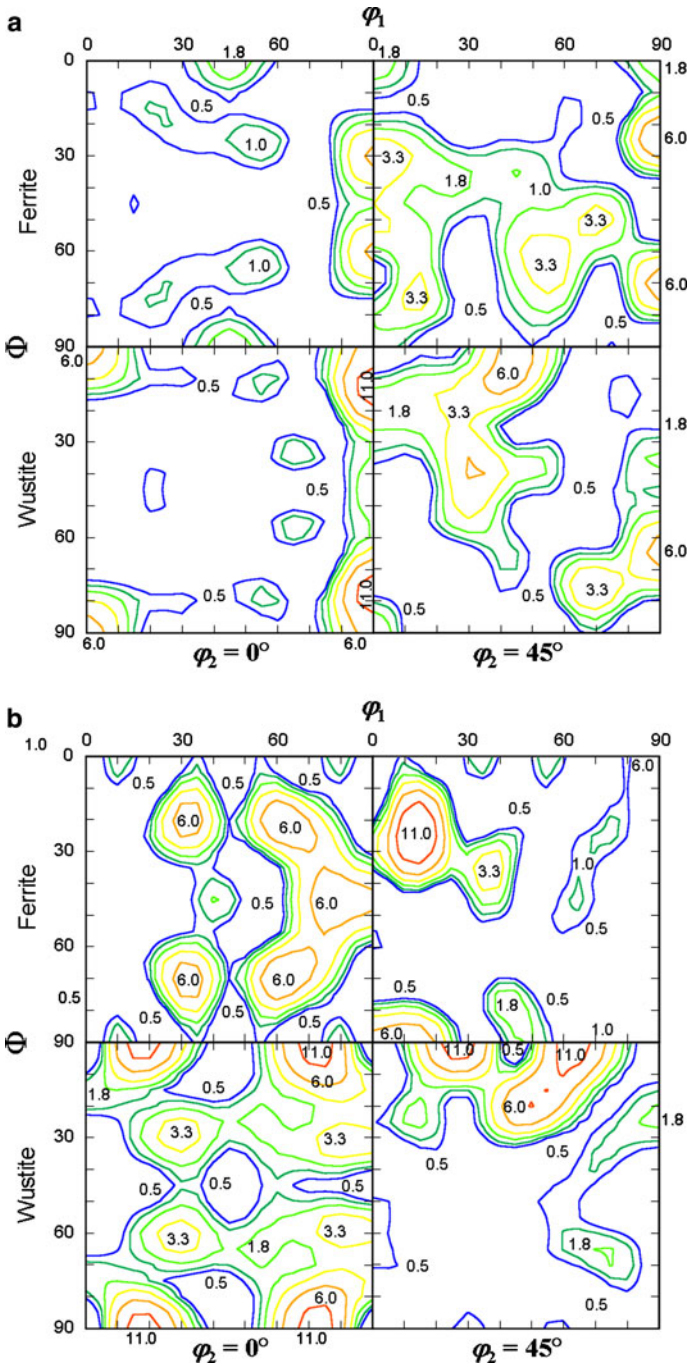
Fig. 9 ODF sections at φ_2 equal to 0 and 45° for wustite and ferrite of the specimens reheated at 1050 °C and cooled to 650 °C that was left undeformed (**a**) and deformed to a 70% reduction in height (**b**)
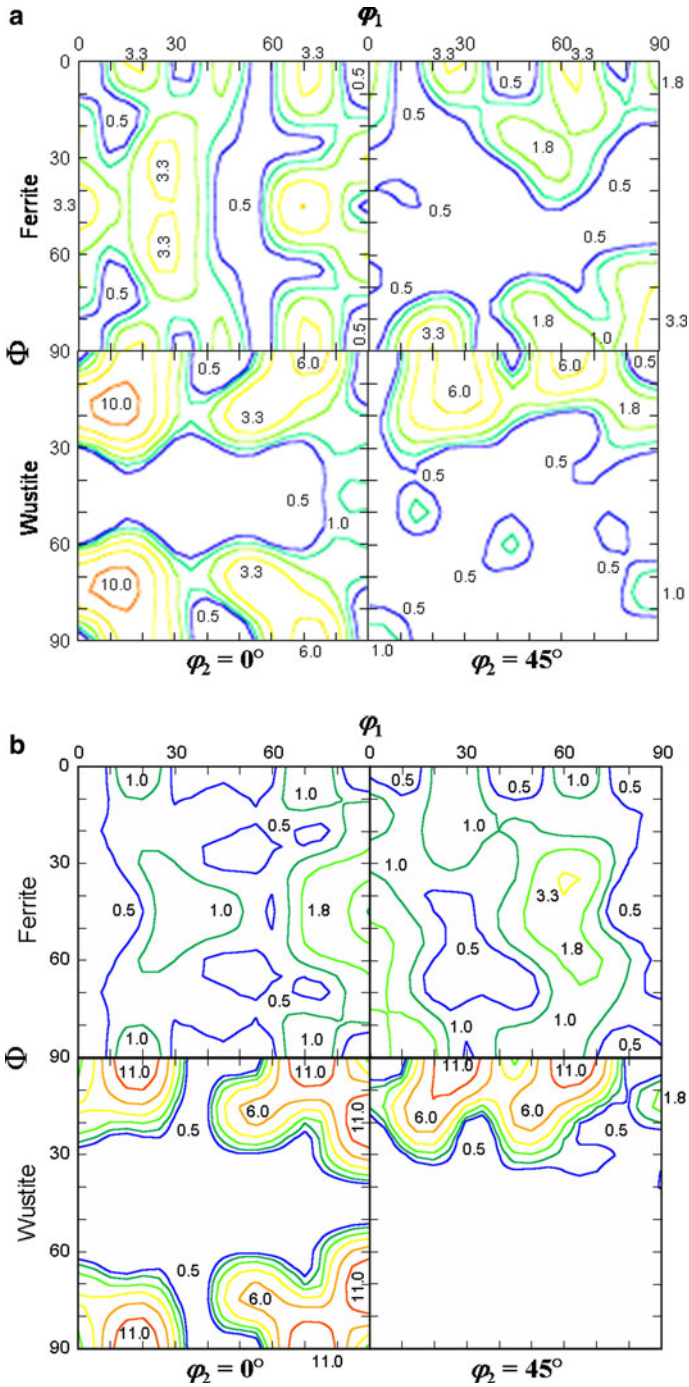
Fig. 10 ODF sections at φ_2 equal to 0 and 45° for wustite and ferrite of the specimens reheated at 1000 °C and left undeformed (a) and hot rolled to a 25% reduction in height (b)
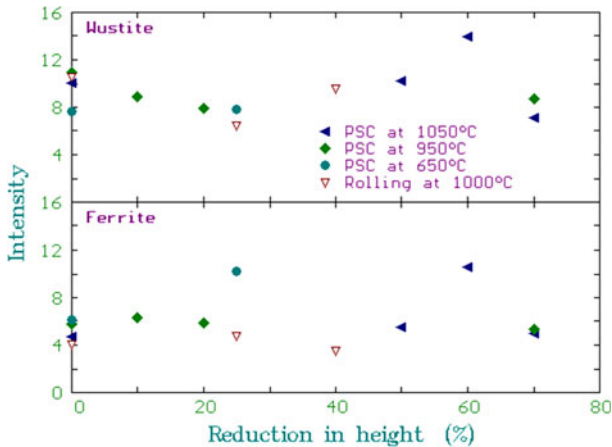
Fig. 11 Values of the maximum component of texture as a function of reduction in height

The highest component of texture in the undeformed sample used in the rolling trials has an intensity above 10 and it is close to $\langle 212 \rangle \{210\}$.

Deformation by plane strain compression or hot rolling does not change the intensity of the components to a high degree, Fig. 11. The effect that deformation exerts on wustite is for the cube components to rotate towards the $\langle 210 \rangle$ direction that lies between the cube and rotated cube components, Figures 7b, 8b and 9b; hot rolled wustite shows the tendency for developing strong $\langle 100 \rangle \{210\}$ components. What is of interest is the high amount of deformation that wustite can sustain at temperatures above 800 °C.

Ferrite does not seem to develop strong texture components by deformation; the solely exception would be that of the specimen that was subjected to a 25% reduction at 650 °C in which a strong component close to $\langle 114 \rangle \{131\}$ is found to occur, Fig. 9b. It is worth mentioning that the specimens that result in fine grained ferrite, Figs. 3b and 6c, do not develop strong texture components, Fig. 10b. The reason for this is that the substrate is made of austenite when deformation is carried out at 950 °C and in the dual phase regime at 800 °C. In any case, transformation to ferrite from austenite results in weak texture components in ferrite [22].

Conclusions

It is found that the oxide layers grown in an experimental chamber for short periods of time at 1050 °C are made entirely of wustite that exhibits a high ductility when deformed in plane strain compression at temperatures above 950 °C. Wustite become fragile and penetrates into the steel substrate when deformed below 700 °C.

The oxide layer grown on a conventional furnace was found to be made of wustite and a thin layer of magnetite. This layer was found to exhibit a more fragile

behaviour when rolled at 1000 °C, and this effect can be attributed to heat conduction from the rolled stock and the work rolls, which will be responsible for reducing the temperature of the oxide layer.

The oxide layer grown in the experimental chamber develops strong cube components that rotate towards $\langle 100 \rangle$ directions when deformed; the final texture lies along the θ-fibre. Ferrite does not develop a strong texture except when deformed at 650 °C.

References

1. M. M. Wolf, *Iron and Steelmaker* **27**, 63 (2000).
2. M. M. Wolf, *Iron and Steelmaker* **27**, 114 (2000).
3. R. Y. Chen and W. Y. D. Yuen, *Oxidation of Metals* **59**, 433 (2003).
4. K. Stanley, J. von Hoene, and R. T. Huntoon, *Transactions ASM* **43**, 426 (1951).
5. F. Païdassi, *Revue de Metallurgie* **54**, 569 (1957).
6. O. Kubaschewsky and B. E. Hopkins, *Oxidation of Metals and Alloys* (Butterworths, London, 1962).
7. N. Birks and A. Nicholson, *Iron Steel Inst. Sp. Pub. 123* (Iron Steel Inst., London, 1970), p. 219.
8. K. W. Browne, J. Dryden, and M. Assefpour, in *Recent Advances in Heat Transfer and Micro-Structure Modelling for Metal Processing*, eds. R.-M. Guo and J. J. Too, MD-vol. 67 (ASME, New York, 1995), p. 187.
9. H. T. Abuluwefa, R. I. L. Guthrie, and F. Ajersch, *Metallurgical and Materials Transactions A* **28A**, 1643 (1997).
10. H. A. Wriedt, in *Binary Alloy Phase Diagrams*, vol. 2, 2nd edn., eds. T. B. Massalski, H. Okamoto, P. R. Subramanian, and L. Kacprzak (ASM International, Metals Park, OH, 1990), p. 1739.
11. Y. Hidaka, T. Anraku, and N. Otsuka, *Oxidation of Metals* **59**, 97 (2003).
12. M. Kryzanowski, C. M. Sellars, and J. H. Beynon, Thermomechanical Processing: Mechanics, Microstructure and Control, eds. E. J. Palmiere, M. Mahfouf, and C. Pinna, (U. Sheffield, Sheffield, 2002), p. 94.
13. D. Filatov, O. Pawelski, and E. Rasp, *Steel Research International* **75**, 20 (2004).
14. L. Suárez, Y. Houbaert, X. Vanden Eynde, and R. Colás, *Corrosion Science* **59**, 309 (2009).
15. R. Y. Chen and W. Y. D. Yuen, *ISIJ International* **45**, 52 (2005).
16. D. P. Burke and R. L. Higginson, *Scripta Materialia* **42**, 277 (2000).
17. B. Kim and J. A. Szpunar, *Scripta Materialia* **44**, 2605 (2001).
18. R. L. Higginson, B. Roebuck, and E. J. Palmiere, *Scripta Materialia* **47**, 337 (2002).
19. S. I. Wright, B. L. Adams, and K. Kunze, *Metallurgical Transactions A* **24A**, 819 (1993).
20. F. J. Humphreys, *Journal of Materials Science* **36**, 3833 (2001).
21. H. J. Bunge, *Texture Analysis in Materials Science* (Butterworths, London, 1982).
22. R. K. Ray, J. J. Jonas, M. P. Butrón-Guillén, and J. Savoie, *ISIJ International* **34**, 927 (1984).
23. D. Duly, G. J. Baxter, H. R. Shercliff, J. A. Whiteman, C. M. Sellars, and M. F. Ashby, *Acta Materialia* **44**, 2947 (1996).
24. L. Suárez, Y. Houbaert, X. Vanden Eynde, and R. Colás, *Oxidation of Metals* **70**, 137 (2008).
25. A. Airod, H. Vandekinderen, J. Barros, R. Colás, and Y. Houbaert, *Journal of Materials Processing Technology* **134**, 398 (2003).
26. P. R. Calvillo, T. Ros-Yanez, D. Ruiz, R. Colás, and Y. Houbaert, *Materials Science and Technology* **22**, 1105 (2006).
27. L. Suárez, Y. Houbaert, X. Vanden Eynde, and R. Colás, *Corrosion Science* **59**, 309 (2009).
28. R. Colás, *Modelling and Simulation in Materials Science and Engineering* **3**, 437 (1995).
29. M. Torres and R. Colás, *Journal of Materials Processing Technology* **105**, 258 (2000).

30. L. Suárez, *Growth and Deformation Behaviour of Oxide Scales on Steel*, Ph.D. Thesis, University of Ghent, Belgium, 2007.
31. U. F. Kocks and H. Mecking, *Acta Metallurgica* **29**, 1865 (1981).
32. T. Sakai and J. J. Jonas, *Acta Metallurgica* **32**, 189 (1984).